# SUPPLEMENTARY INFORMATION

## Correlating mechanism, kinetics, and SEI formation of boron-doped graphene anode for high-performance alkali ion batteries

Surishi Vashishth[1‡], Ujjwal Vidyarthi[1‡], Abhishek Garg[1], Swaraj Servottam[1], M. Eswaramoorthy[1,#,*]

---

### 1. Characterization techniques:

Powder X-ray diffraction (PXRD) analysis of the Cu foil was recorded with a PANalytical diffractometer (Empyrean) having monochromatic Cu $K_{\alpha 1}$ radiation ($\lambda = 1.5404$ Å) with an accelerating voltage of 40 kV and current of 40 mA. Thermogravimetric analysis (TGA) was done with a Mettler Toledo TGA-850 TG analyzer at the ramping rate of 5°C $min^{-1}$ in an oxygen atmosphere. Raman spectra were obtained from Renishaw equipped with a green laser (532 nm). Brunauer–Emmett–Teller (BET) analysis for $N_2$ (ultra-high purity of 99.9995%) sorption studies were conducted at 77 K by Autosorb-i$Q_2$, and samples were degassed for 12 h at 423K. JEM 2100 PLUS electron microscope of 200 KV was used to acquire the samples' transmission electron microscope (TEM) images. ZEISS GEMINI 500 was used to procure field emission scanning electron microscopy (FESEM) images. X-ray photoelectron spectroscopy (XPS) measurements were carried out by an X-ray photoelectron spectrometer (Thermo K-alpha+) using micro-focused and monochromated AlKα radiation with energy 1486.6 eV. The FESEM, TEM, and XPS samples were prepared by sonicating the powdered sample in 99.99% pure ethanol and uniformly drop casting on Cu foil, Cu grid, and Si wafer, respectively. Battery cycler Biologic BCS-810 was used for battery studies.

### 2. Electrochemical Characterization:

BTEG electrode was prepared by slurry (containing 80 wt% BTEG, 10 wt% Vulcan carbon XC-72, and 10 wt% polyvinylidene fluoride (PVDF) casting on copper foil with blade coating technique and dried at 80°C vacuum oven for at least 24 h, keeping mass loading of 1.27 mg $cm^{-2}$. TEG-350 and TEG pellets were prepared by the cold press with 17 mg weight per pellet of sample. BTEG i.e., active material loading was 1 mg with a 10 mm diameter. The electrochemical performance of BTEG and controls was evaluated in the Swagelok cell. BTEG was used as a working electrode and lithium, sodium, and potassium foil was used as counter (reference) electrode of 11mm diameter. 1M $LiPF_6$, 1M $NaPF_6$, 0.8M $KPF_6$, and 5M KFSI in ethylene carbonate: diethyl carbonate (1:1 by volume) for LIB, SIB, and PIB respectively. The electrolytes were allowed to stir for at least 24 hours and 120 μl was added to the separator.

For the symmetric cell studies, 11mm metal foils were used as electrodes, with Whatman filter Glass fibre paper as a separator. A single separator was used for Li, Na, while two separators for K symmetric cells. The charge-discharge current was set 9.55μA, with charging and discharging preformed for 1 hour each. Pre-cycling was conducted to assess its impact on enhancing the initial Coulombic efficiency (ICE). For the Li/Na/K pre-treatment, a half-cell was initially assembled and subjected to a single discharge cycle at a current density of 25 mA $g^{-1}$. Following this, the cell was disassembled, the metal foil (11 mm) was replaced, and a new separator (12 mm) soaked with 100 μL of electrolyte was inserted. The reassembled cell underwent cycling at 25 mA $g^{-1}$ for five cycles, after which the current density was increased to 1 A $g^{-1}$. The BTEG electrodes (10 mm) were prepared with a consistent composition of 80 wt% BTEG, 10 wt% Vulcan carbon XC-72, and 10 wt% polyvinylidene fluoride (PVDF). The electrolytes used were: for LIBs, 1 M $LiPF_6$ in EC:DEC (1:1 by volume); for SIBs, 1 M $NaPF_6$ in EC:DEC:FEC (10:10:1 by volume); and for PIBs, 5 M KFSI in EC:DEC (1:1 by volume). Cyclic voltammetry (CV), galvanostatic charge-discharge (GCD), and electrochemical impedance spectroscopy (EIS) tests were conducted on an electrochemical workstation (battery cycler) at room temperature (25°C). Electrochemical impedance spectroscopy was measured on an electrochemical workstation (VMP3, Biologic) in the frequency range from 600kHz and 10mHz with a sinusoidal voltage amplitude of 10mV. All measurements were conducted in ambient conditions. LIB, SIB, and PIB were allowed to equilibrate for 24 hours before testing for CV, GCD, and EIS.

## 3. In-Situ Raman cell

Optical cell configuration (El-Cell ECC-Opto-Std) was used in this study. *In situ,* optical images, taken with 50× magnitude, BTEG as the working electrode was observed through the glass, the copper mesh was used as a current collector on top of BTEG, glass fiber was used as a separator, Li/Na/K foil as the counter electrode. BTEG: CMC (9:1) 10mg of total pellet and Alkali metal foil of diameter 9mm and separator of diameter 10mm was used. Green laser (532nm) was used with laser power of 5% with 30 seconds exposure and 3 times accumulation. Data was recorded every 20 minutes, to avoid burning of the sample due to continuous exposure to the laser. It was scanned at 5 mA $g^{-1}$ to attain homogeneous evolution of the D and G band due to the use of high loading of the pellet.

## 4. Full Cell Fabrication

### 4.1 Materials used for full cell fabrication:

Non-carbon-coated LFP was purchased from Sigma-Aldrich (Product No. 759546, >97% (XRF)), and super C45 was procured from MTI Corporation (SKU: Lib-SC45). The electrolyte used is 1M LiPF6 in EC DEC (1:1 v/v) with 20 ppm of water content, and its colour is light yellow. N-methyl-2-pyrrolidone (NMP) was used with 60 ppm of water content.

### 4.2 Electrochemical Measurements for full cell:

For the preparation of cathode, firstly the LFP and the Super C45 were initially ball-milled in 85:15 weight ratio using a high-energy ball mill (SPEX 8000M) for 15 minutes. Prior to use, Super C45 was dried under vacuum at 110 °C overnight to remove moisture. The cathode slurry was then prepared by mixing Super C45 and LFP, with PVDF in NMP (the weight of PVDF was taken in such a way that the weight ratio becomes 80:10:10) followed by manual grinding in a mortar pestle for 30 minutes. The resulting slurry was casted onto carbon-coated aluminium foil and dried under vacuum in a stepwise manner: initially at 40 °C for 2 h, then at 60 °C for 2 h, and finally at 80 °C for 12 h. After drying, the oven was switched off and allowed to cool to 50 °C before releasing the vacuum, and the electrodes were punched into 10 mm diameter discs. The electrodes were weighed and transferred to the glove box. The mass loading of the active material was maintained between 5.1–5.2 mg cm$^{-2}$. Swagelok cells were used in the fabrication of the full cells. Fabrications were carried out with pre-lithiated electrodes, Whatman filter paper (GF/D) as separator, and 1 M $LiPF_6$ solution in (EC/DEC 1:1 vol%) as electrolyte, inside Argon-filled MBraun glove box with $H_2O < 0.1$ ppm, $O_2 < 0.1$ ppm.

Prior to full-cell assembly, pre-lithiation of both the electrodes, BTEG anode and LFP cathode were carried out through three charge–discharge cycles. For anode, cycling was performed at a current density of 100 mA g$^{-1}$ in voltage range of 3.0–0.01 V with 100 µL of electrolyte, while for the cathode, cycling was done at a C/5 rate (1C = 159.79 mA/g) between 4.0–2.0 V with 200 µL of electrolyte. **Figure S43** shows the charge-discharge profile of the anode and cathode for the third cycle. Following pre-lithiation, the half-cells were disassembled, and the electrodes were further used in the full cell.

Subsequently, full cells were assembled using fresh separators and 100 µL of the same electrolyte. The full cells were cycled, with 2 minutes of rest after each charge and discharge cycle, between 3.87 V and 1.00 V at a C/5 rate, shown in **Figure S7**, maintaining an N/P ratio of 1.005. The N/P ratio was adjusted by modifying the cut-off voltages in accordance with the method reported by Kasnatscheew et al. [Journal of the Electrochemical Society, 2017, 164(12), A2479]. For cycling performance, the same cell was cycled at a 1C rate, after 10 cycles at a C/5 rate, keeping 2 minutes of rest after each charge and discharge cycle, as shown in **Figure S8.**

The specific capacity is calculated based on the mass of the cathode. The full cell delivers the discharge capacity of 60 mAh $g^{-1}$ after 10 cycles with an initial coulombic efficiency of 73.4%. Cycling performance at 1C rate between potential range of 3.87V to 1V shows average coulombic efficiency of 99.47% and capacity retention of 80% (with respect to initial value of discharge capacity of 47mAh $g^{-1}$) after 100 cycles.

## 5. Raman spectra of liquid electrolyte

500ul of electrolytes, salts, and solvents were transferred into NMR tubes with proper sealing. The red laser was chosen with laser power of 5%, exposure time of 30 seconds, and 3 accumulations.

## 6. Galvanostatic intermittent titration technique:

To gain insights into solid-state diffusion and kinetic analysis of alkali ions, a galvanostatic intermittent titration technique (GITT) was carried out. **Figure S14** shows the GITT potential profiles for alkali ions ($M^+$) with a pulse current of 25 mA $g^{-1}$. The corresponding diffusion coefficients for $M^+$ were calculated based on the following formula: [1]

$D = 4\pi\tau(n_mV_m/S)^2(\Delta Es/\Delta E\tau)^2$ (3)

In this formula, $n_m$, $V_m$, $\tau$, and S represent the mole of the electrode material, molar volume, relaxation time, and electrode-electrolyte contact area, respectively. An enlarged GITT discharge-potential profile is displayed in **Figure S14e**, where ΔEs is the potential change caused by the pulse, and ΔEτ is the potential change for constant current. **Figure 5e** shows the apparent diffusion coefficients of $M^+$ ($D_{M+}$) as a function of potential. The potential change during each relaxation period represents overpotential at the corresponding insertion/extraction stage.[2] The coefficients were calculated at all steps during the GITT measurements except for the 1st step and the end two steps due to the large voltage variations.

## 7. Figures:

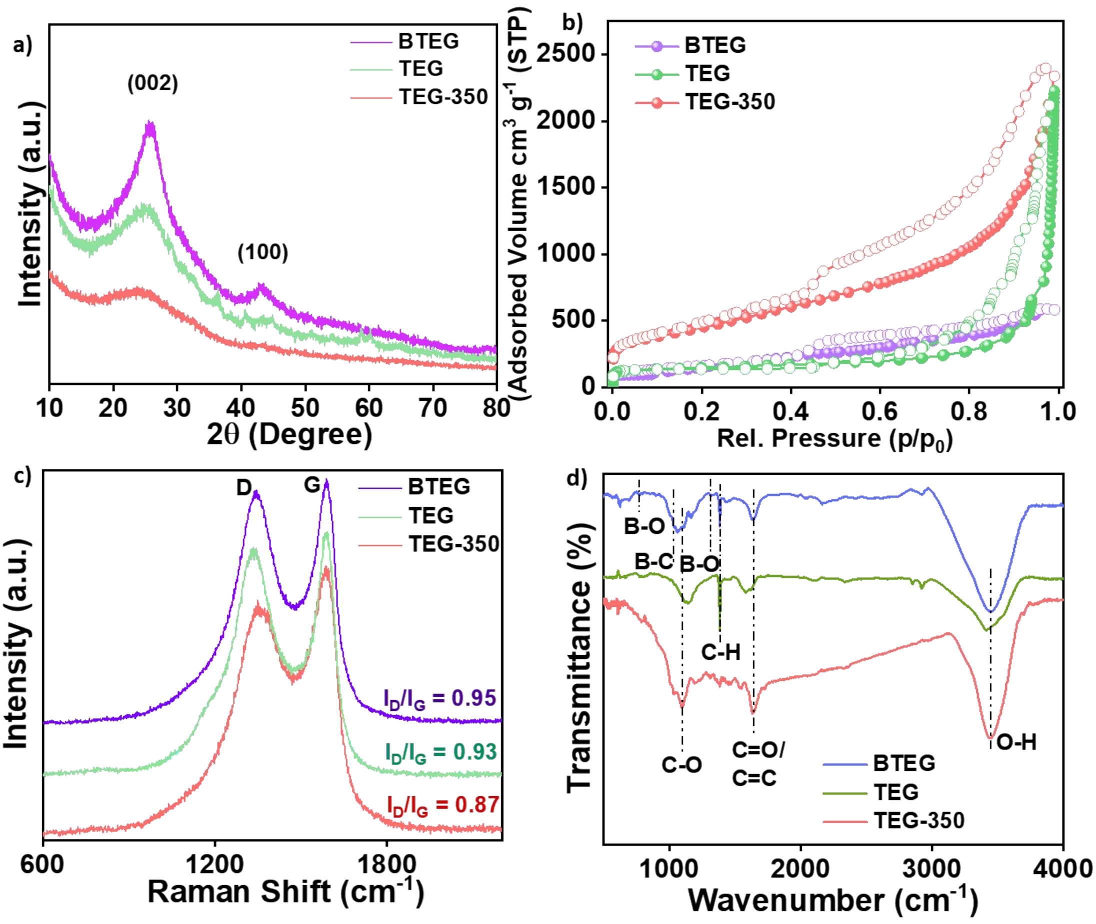

**Figure S1.** a) PXRD, b) BET, c) Raman spectra and d) FT-IR is compared for BTEG, TEG and TEG-350.

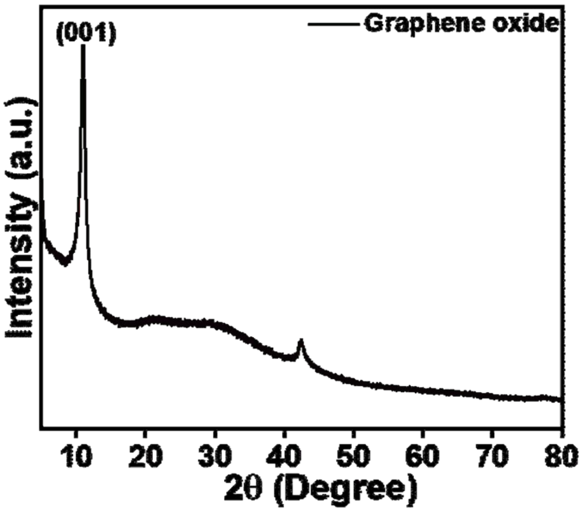

**Figure S2.** Thermogravimetric curve of BTEG in oxygen atmosphere suggests 12wt% of $B_2O_3$.

TGA Calculations:

Boron wt.% = (100-weight loss)% / molecular weight of boron * molecular weight of boric acid

= 12%/ 69.62 * 21.62

= 3.7wt.%

a)

| B-species | BTEG (%) |
|---|---|
| **B-OH** | 3.28 |
| **$BCO_2$** | 51.12 |
| **$BC_2O$** | 41.12 |
| **$BC_3$** | 4.39 |

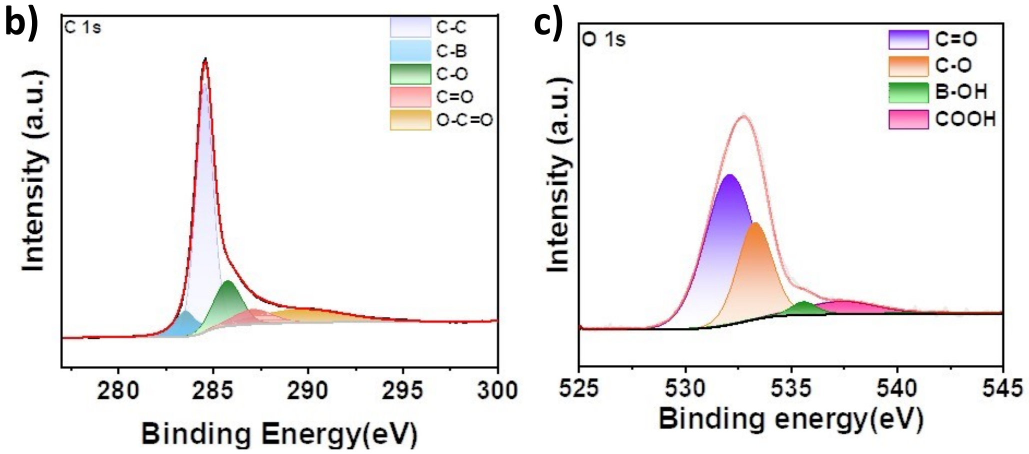

**Figure S3. a)** Content of different boron species (%), X-ray photoelectron spectroscopy **b)** C1s and **c)** O1s spectra of BTEG

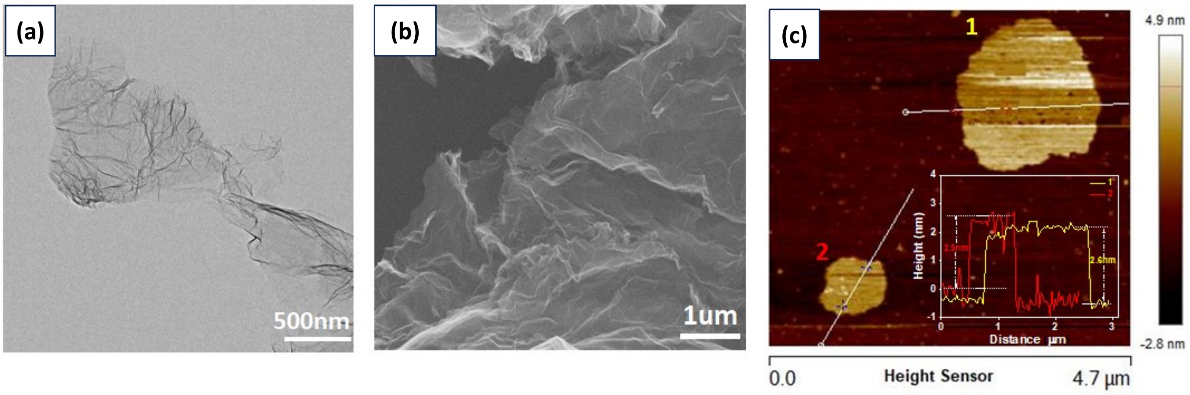

**Figure S4.** Microscopy images of BTEG and TEG. **a)** TEM image of TEG **b)** SEM image of BTEG and **c)** AFM image of BTEG.

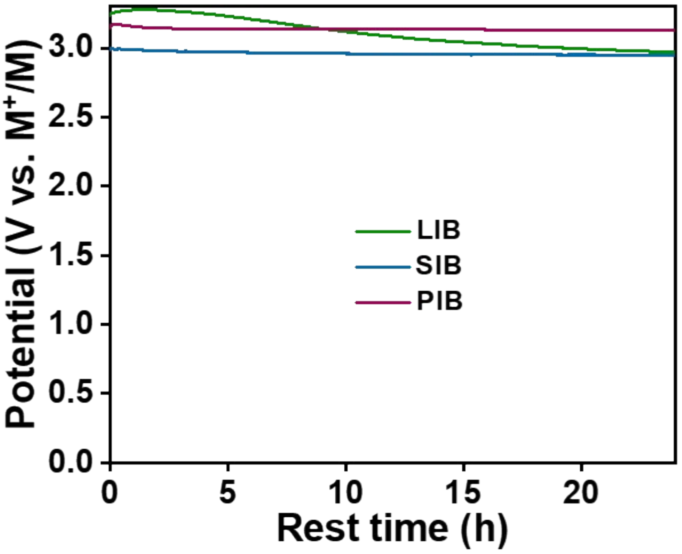

**Figure S5.** Comparison of OCV curves for half-cell with BTEG for 24 hours in case of lithium-ion (1M $LiPF_6$ in EC:DEC), sodium-ion (1M $NaPF_6$ in EC:DEC:FEC) and potassium-ion (5M KFSI in EC:DEC) battery.

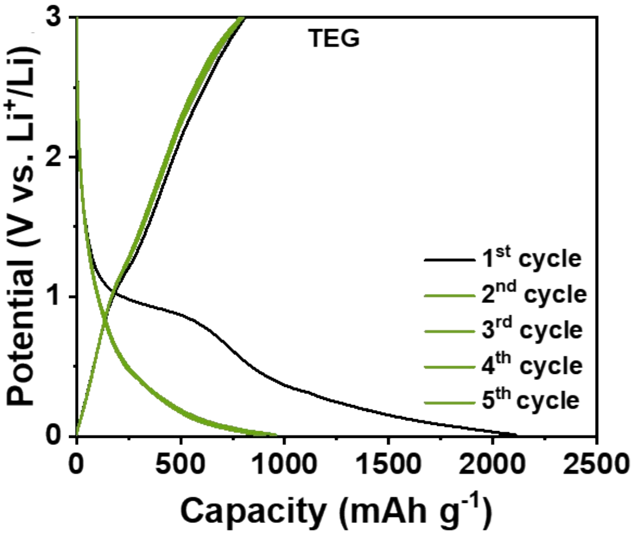

**Figure S6.** Charge-discharge profile of TEG at 25mA $g^{-1}$ for LIB.

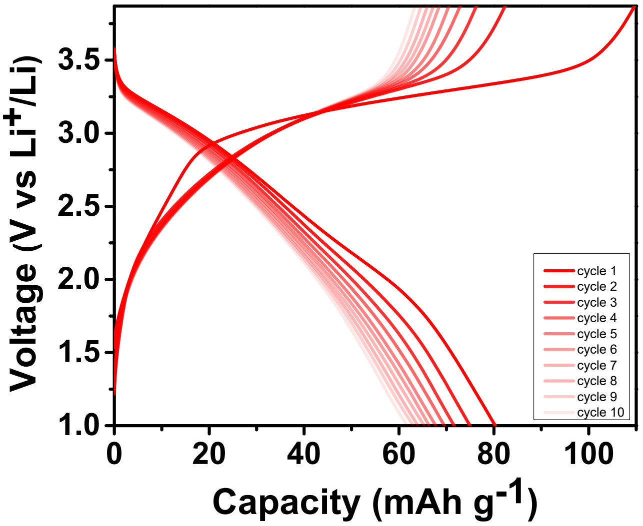

**Figure S7.** Charge–discharge profile of the full cell measured at a rate of C/5 within a voltage window of 3.87–1.00 V.

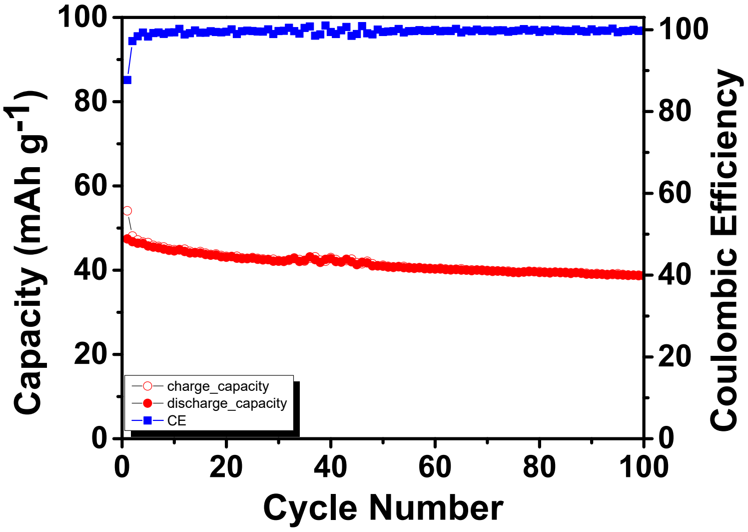

**Figure S8.** Cycling performance of the full cell measured at a rate of C/1 within a voltage window of 3.87–1.00 V.

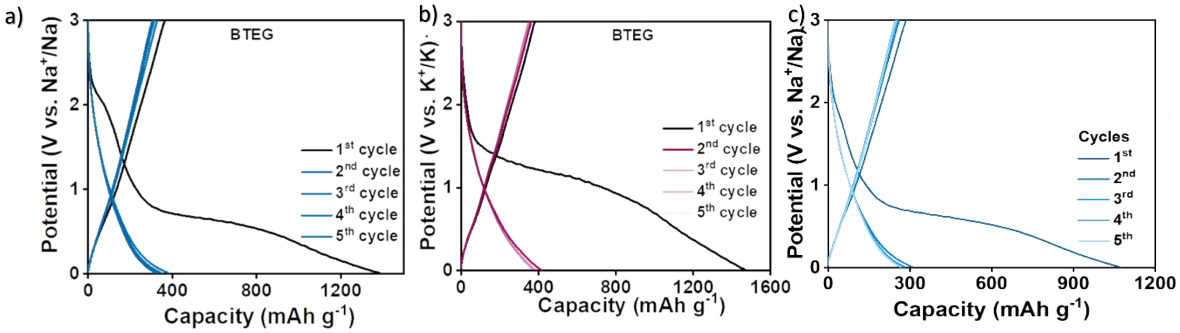

**Figure S9.** Charge discharge profile of BTEG at 25mA g$^{-1}$ for **a)** SIB (1M $NaPF_6$ EC: DEC: FEC), **b)** PIB (5M KFSI EC: DEC) up to 5 cycles and **c)** galvanostatic charge-discharge for BTEG with 1M $NaPF_6$ EC: DEC.

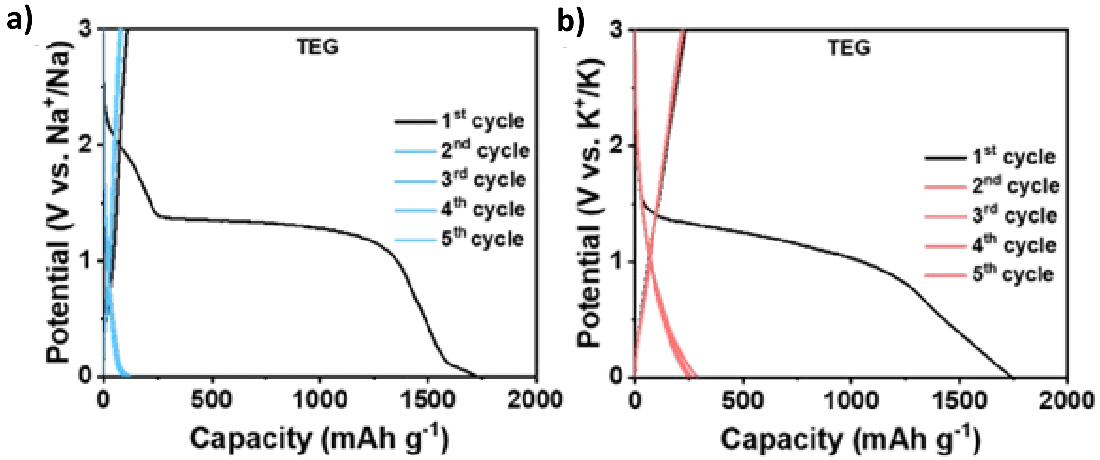

**Figure S10.** Charge-discharge profile of TEG at 25mA g$^{-1}$ for **a)** SIB (1M $NaPF_6$ EC: DEC: FEC) and **b)** PIB (5M KFSI EC: DEC) up to 5 cycles.

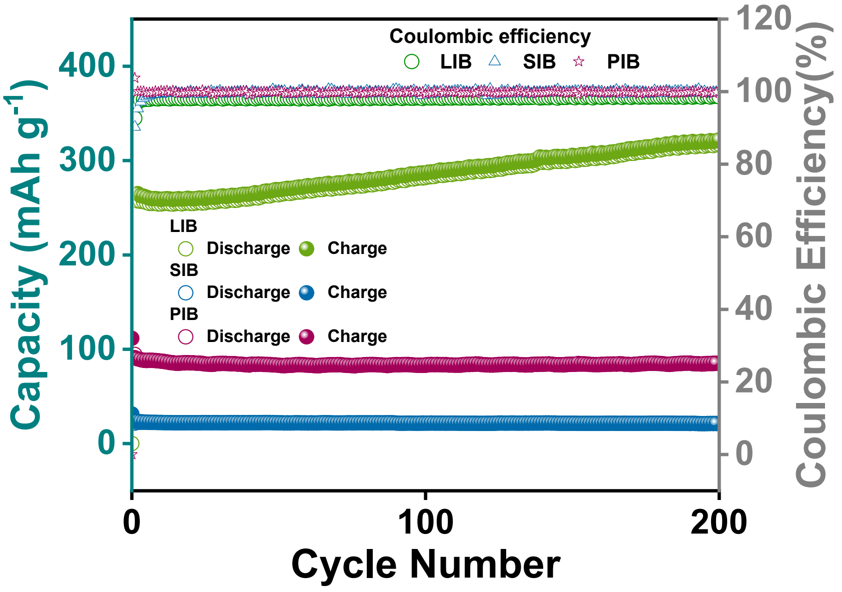

**Figure S11.** Charge discharge of TEG for Li, Na and K ion battery.

| SIB<br>Current density (mA $g^{-1}$) | BTEG<br>(Capacity, mAh $g^{-1}$) | TEG<br>(Capacity, mAh $g^{-1}$) |
|---|---|---|
| 25 | 295 | 83 |
| 100 | 246 | 38 |
| 200 | 220 | 27 |
| 500 | 195 | 18 |
| 800 | 172 | 13 |
| 1000 | 154 | 12 |
| 25 | 272 | 70 |

**Table S1**. Comparison of rate performance between BTEG and TEG for SIB.

| PIB<br>Current density (mA $g^{-1}$) | BTEG<br>(Capacity, mAh $g^{-1}$) | TEG<br>(Capacity, mAh $g^{-1}$) |
|---|---|---|
| 25 | 369 | 225 |
| 100 | 283 | 191 |
| 200 | 246 | 158 |
| 500 | 211 | 129 |
| 800 | 189 | 113 |

|  |  |  |
|---|---|---|
| 1000 | 182 | 105 |
| 25 | 331 | 211 |

**Table S2.** Comparison of rate performance between BTEG and TEG for PIB.

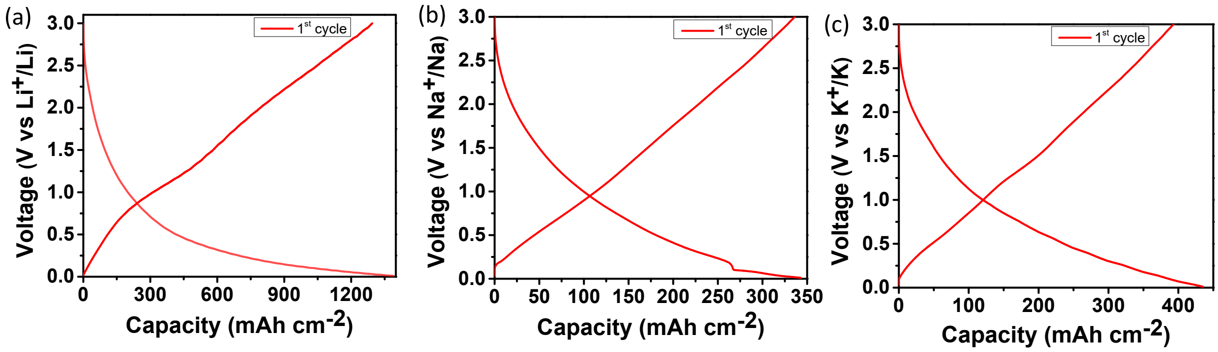

**Figure S12.** First charge-discharge profile with **(a)** pre-lithiation, **(b)** pre-sodiation, **(c)** pre-potassiation.

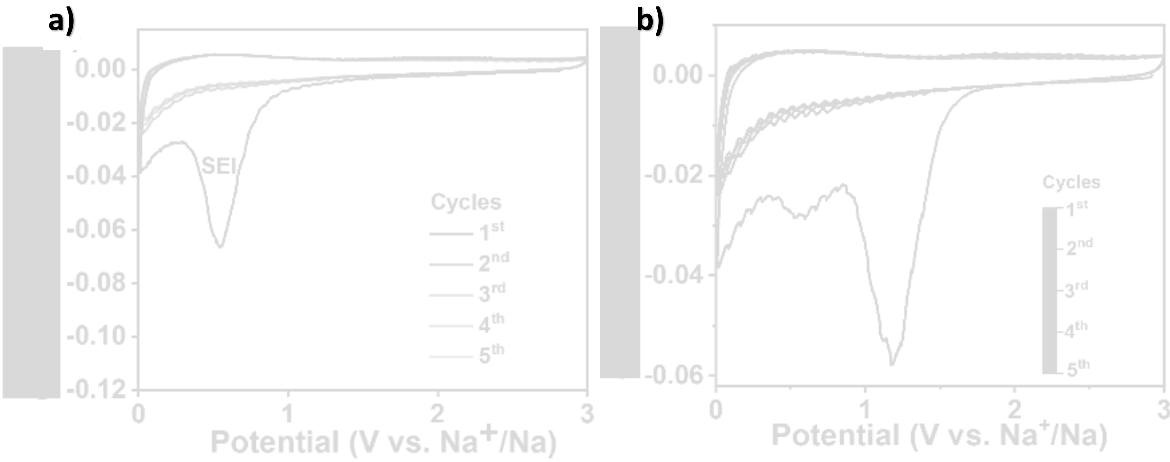

**Figure S13.** CV scan for BTEG with **a)** 1M $NaPF_6$ EC: DEC and **b)** 1M $NaPF_6$ EC: DEC: FEC.

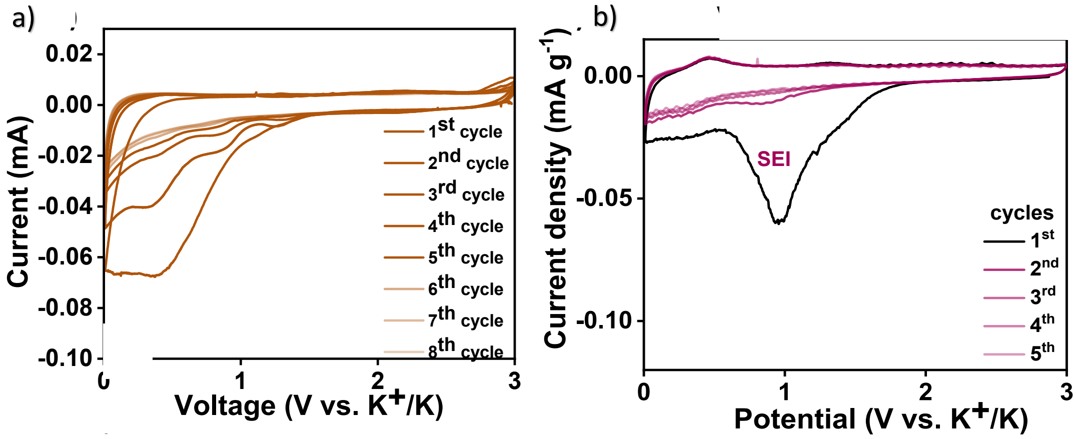

**Figure S14.** The electrochemical properties of BTEG// K half-cell. CV curves at a scan rate of 0.01mV s$^{-1}$ (0.01-3.0V) for **a)** PIB (0.8M $KPF_6$), and **b)** PIB (5M KFSI)

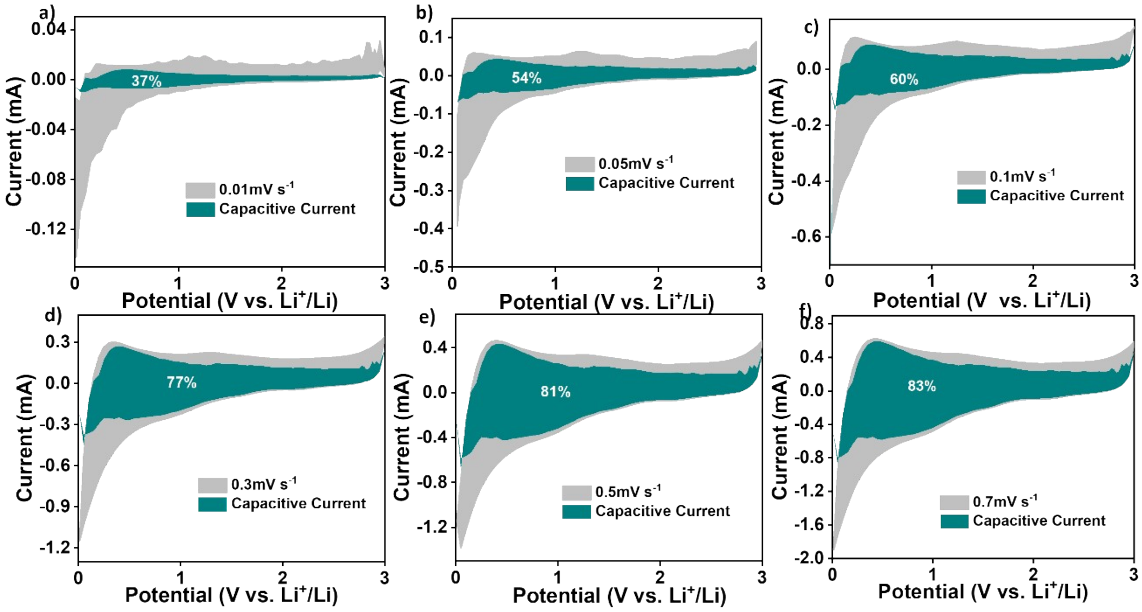

**Figure S15.** Pseudocapacitive contribution for BTEG//Li half-cell at a) 0.01mV s$^{-1}$, b) 0.05mV s$^{-1}$, c) 0.1mV s$^{-1}$, d) 0.3mV s$^{-1}$, e) 0.5mV s$^{-1}$ and f) 0.7mv s$^{-1}$.

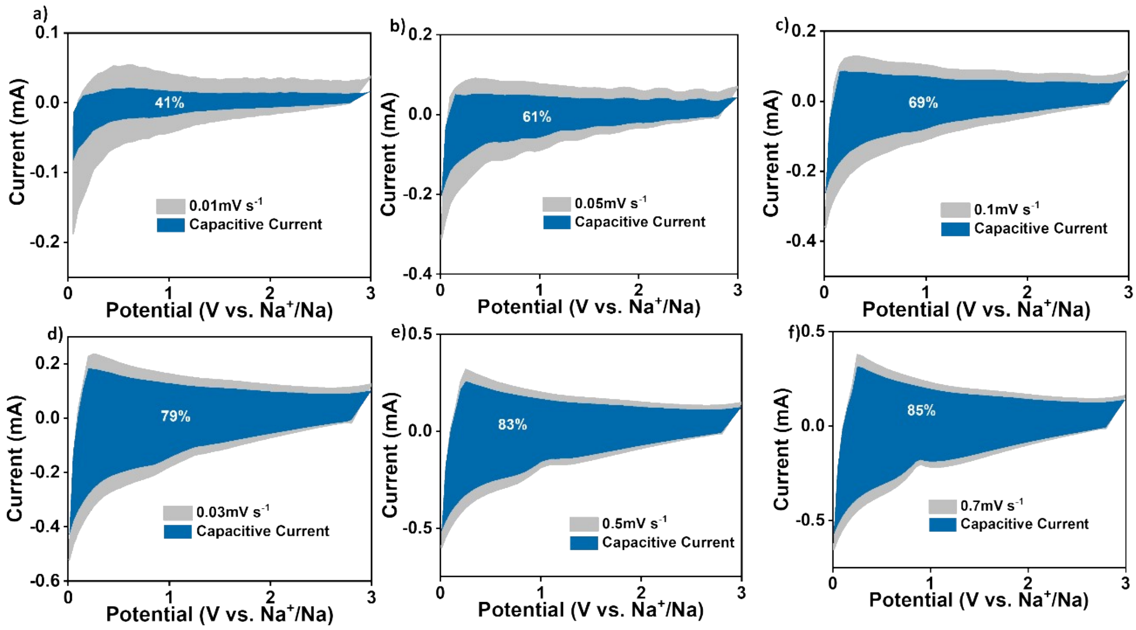

**Figure S16.** Pseudocapacitive contribution for BTEG//Na half-cell at a) 0.01mV s$^{-1}$, b) 0.05mV s$^{-1}$, c) 0.1mV s$^{-1}$, d) 0.3mV s$^{-1}$, e) 0.5mV s$^{-1}$ and f) 0.7mv s$^{-1}$.

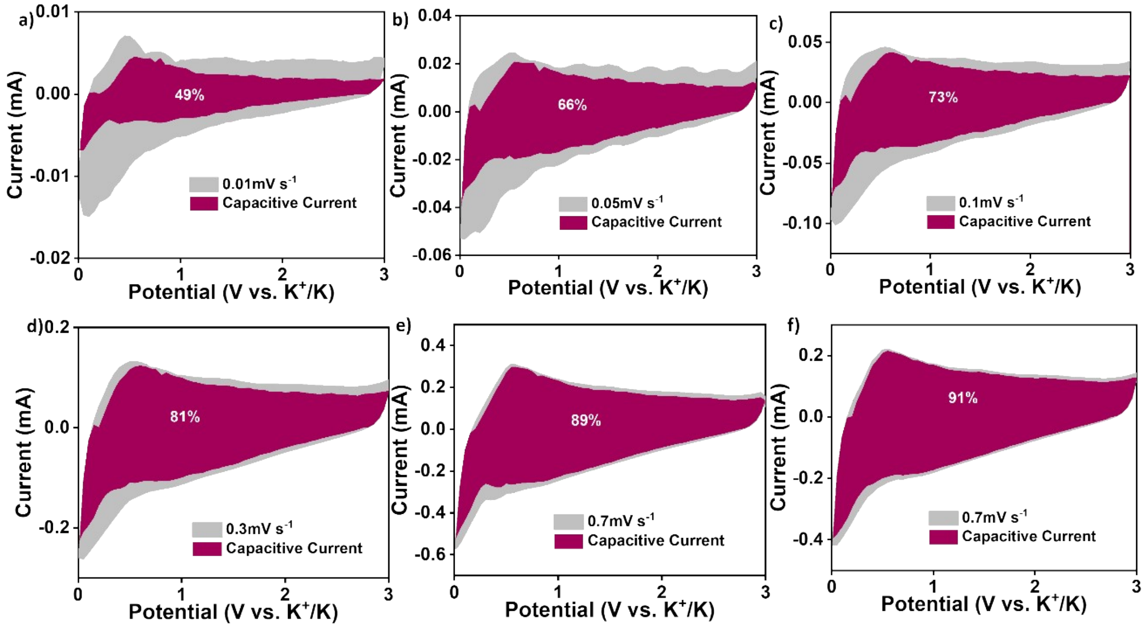

**Figure S17.** Pseudocapacitive contribution for BTEG//K half-cell at a) 0.01mV s$^{-1}$, b) 0.05mV s$^{-1}$, c) 0.1mV s$^{-1}$, d) 0.3mV s$^{-1}$, e) 0.5mV s$^{-1}$ and f) 0.7mv s$^{-1}$.

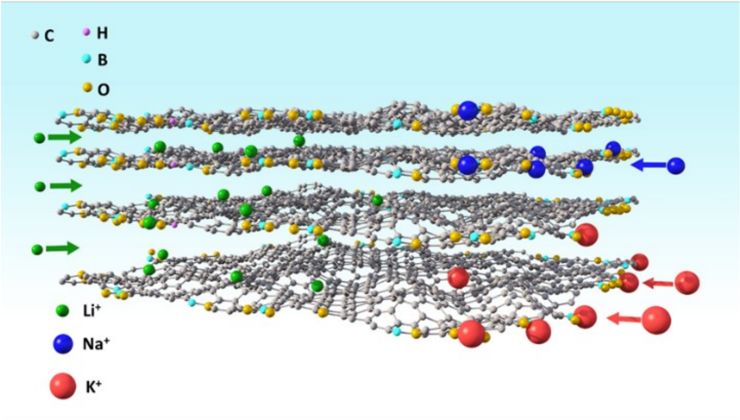

**Figure S18.** Schematic illustration of proposed reaction mechanism of BTEG anode for LIB, SIB and PIB.

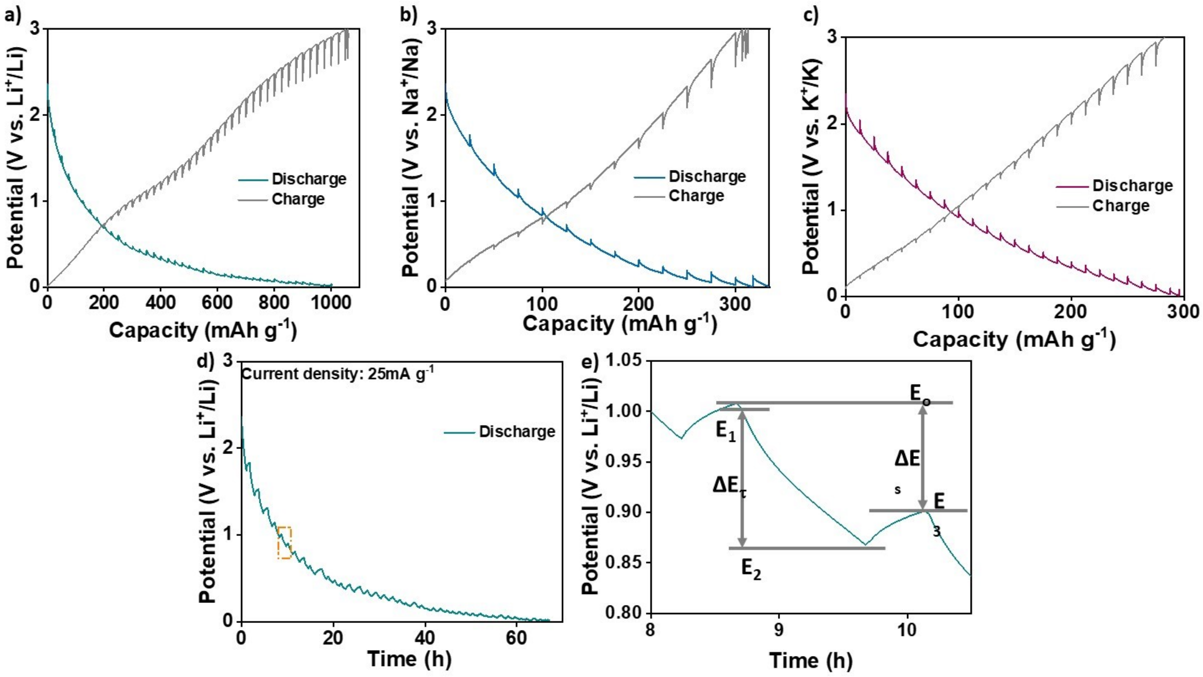

**Figure S19.** Charge discharge with potential profile for GITT measurement for a) LIB, b) SIB and c) PIB. The enlarged GITT graph of e) BTEG//Li in discharge process as the example: ΔEτ is the voltage change of constant current discharging which is calculated by the equal $E_1$ -$E_2$; ΔEs is the voltage change caused by the pulse which is calculated by the equal $E_0$ -$E_3$ .

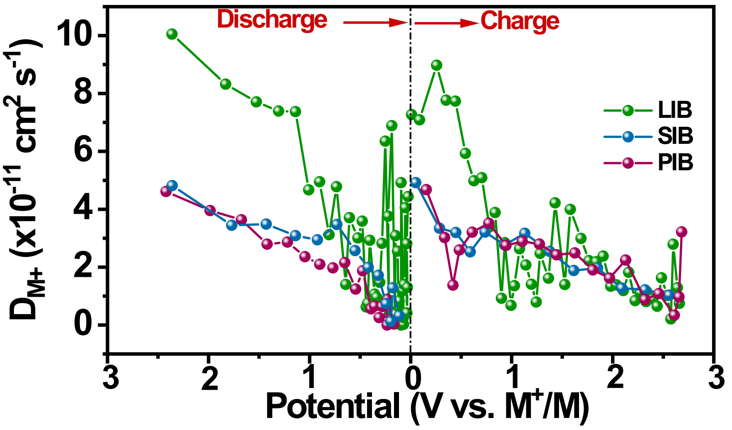

**Figure S20.** Comparison of diffusion coefficient values of LIB, SIB and PIB with BTEG electrode during discharging and charging.

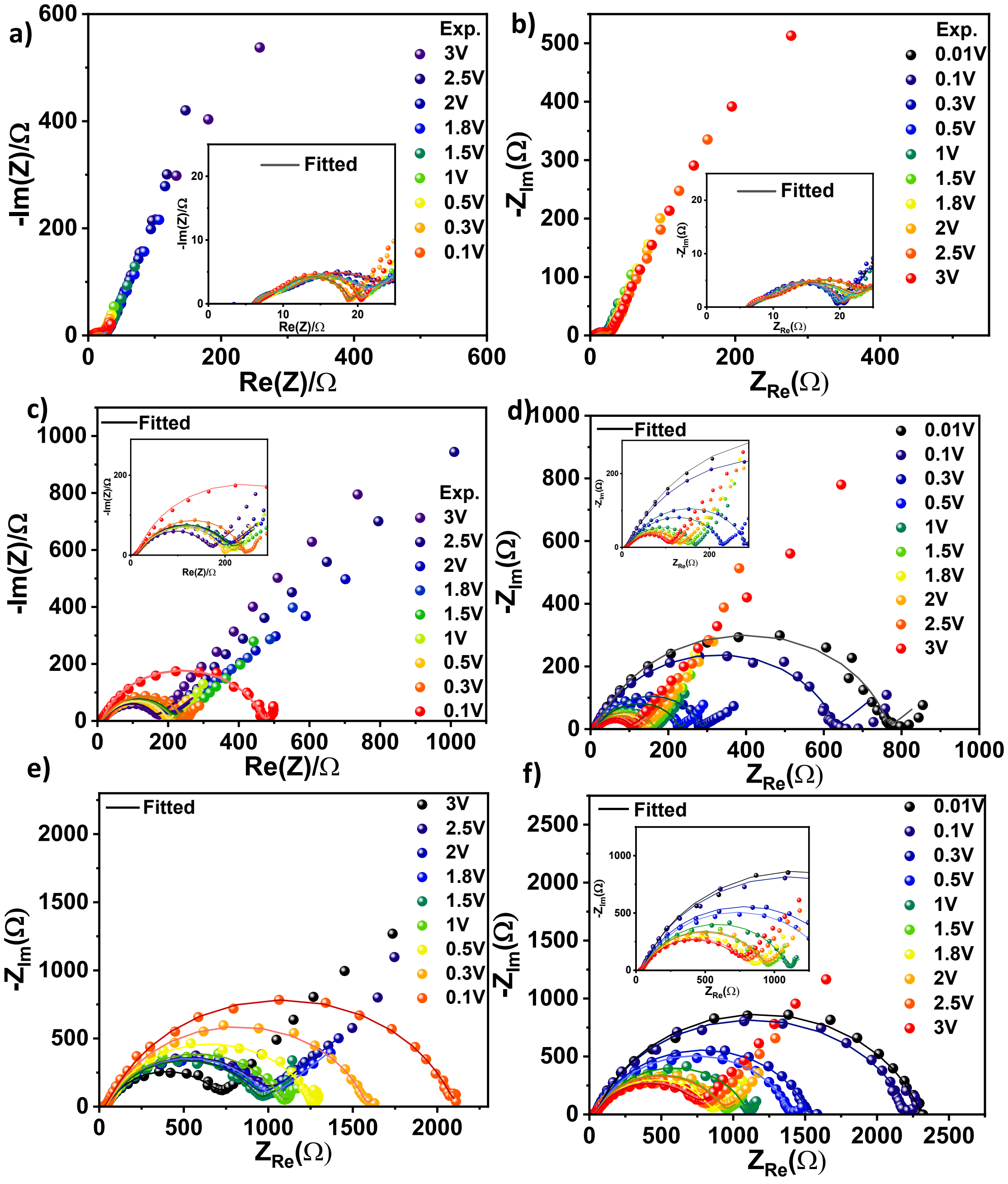

**Figure S21.** In-situ impedance fitted data with experimental data for discharge/ charge for (a,b) LIB, (c,d) SIB and (e,f) PIB.

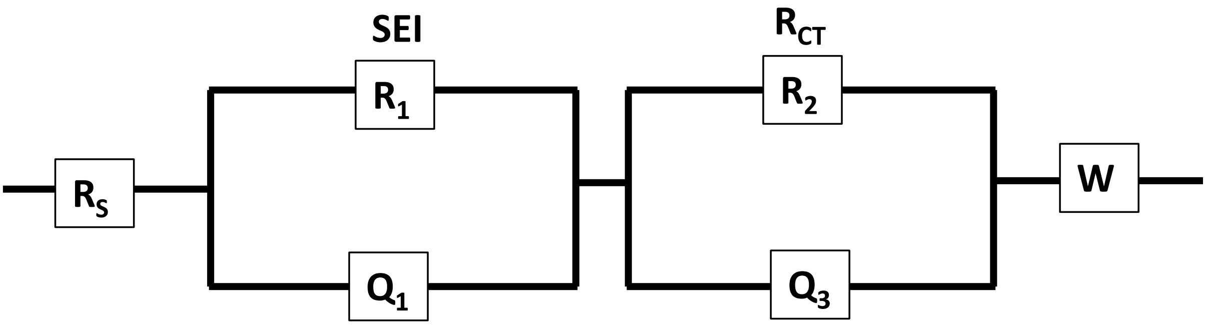

**Figure S22.** Equivalent circuit corresponding to Nyquist plot showing three types of resistance i.e., solution, SEI and charge transfer.

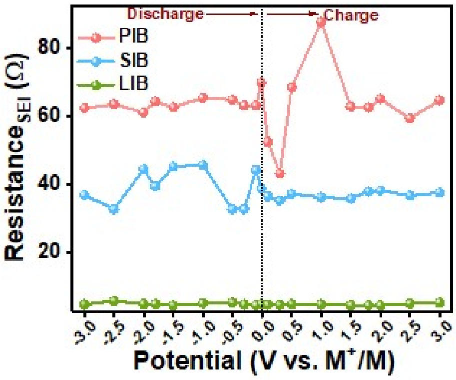

**Figure S23.** Resistance associated with solid electrolyte interphase ($R_{SEI}$) component for BTEG in LIB(green), SIB(blue) and PIB(peach).

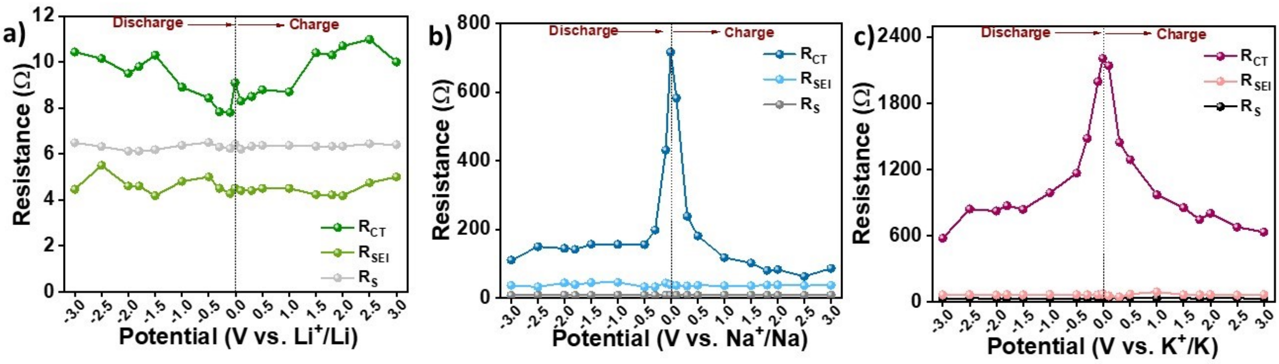

**Figure S24**. Resistance components in a) LIB, b) SIB and c) PIB.

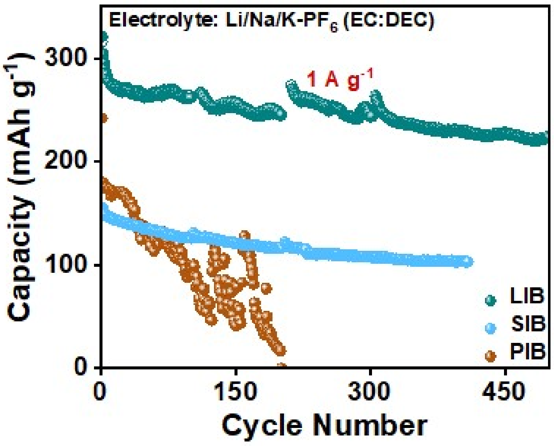

**Figure S25.** Long term stability of BTEG in 1M $LiPF_6$, 1M $NaPF_6$ and 0.8M $KPF_6$ (EC:DEC) at 1A $g^{-1}$.

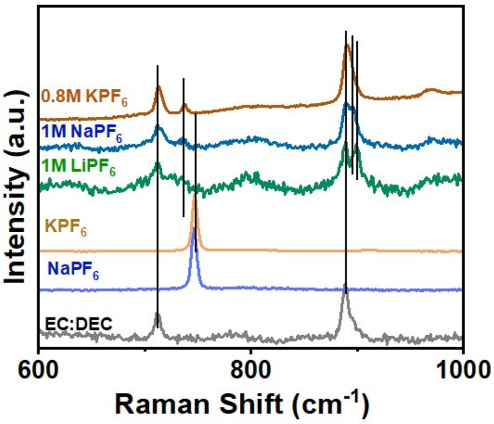

**Figure S26.** Raman spectra of 1M $LiPF_6$, 1M $NaPF_6$, 0.8M $KPF_6$ (EC:DEC) electrolytes, $NaPF_6$, $KPF_6$ salt and EC: DEC solvent.

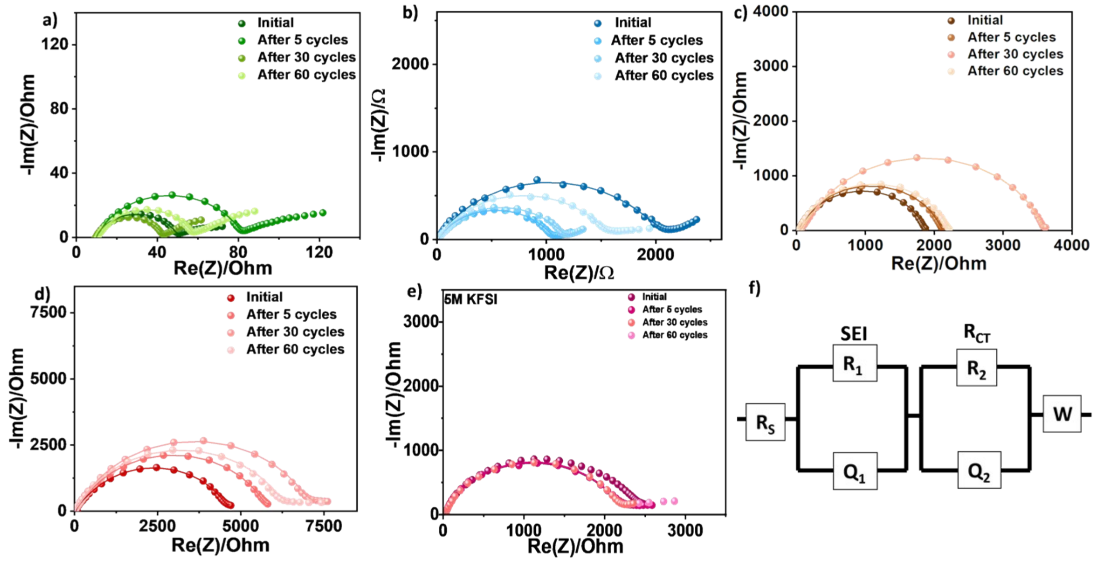

**Figure S27.** Nyquist plots for symmetric cells with **a)** 1M $LiPF_6$, **b)** 1M $NaPF_6$, **c)** 0.8M $KPF_6$, **d)** 1M KFSI, **e)** 5M KFSI in EC: DEC and **f)** equivalent electrical circuit used for fitting the impedance spectra.

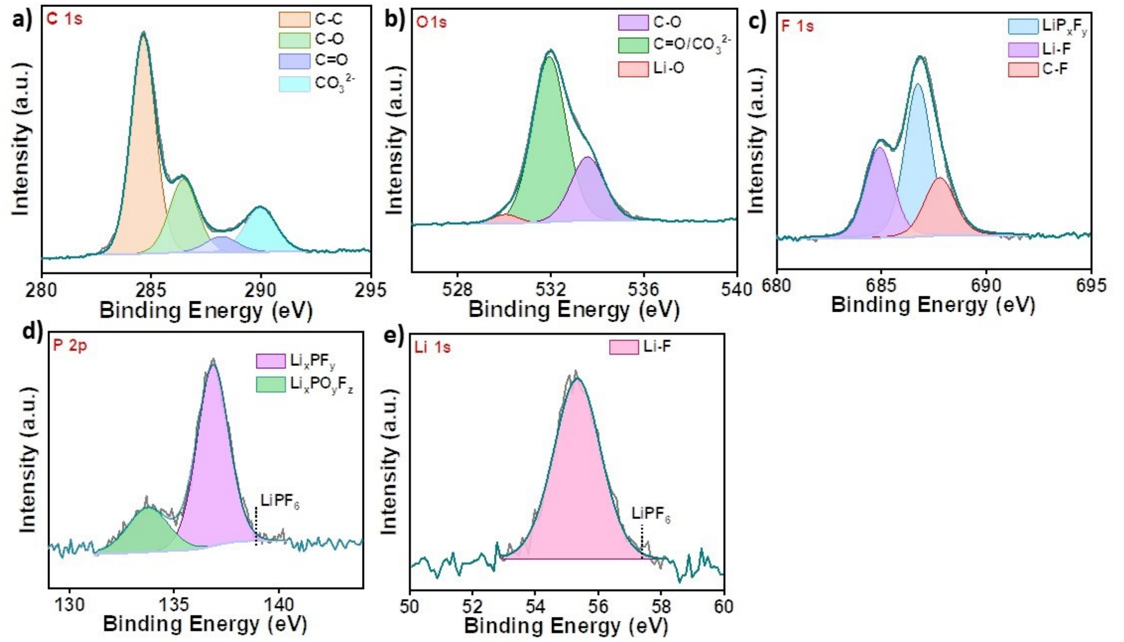

**Figure S28.** XPS spectra BTEG in 1M $LiPF_6$ (EC: DEC) before etch for elements a) C1s, b) O1s, c) F1s, d) P 2p and e) Li 1s.

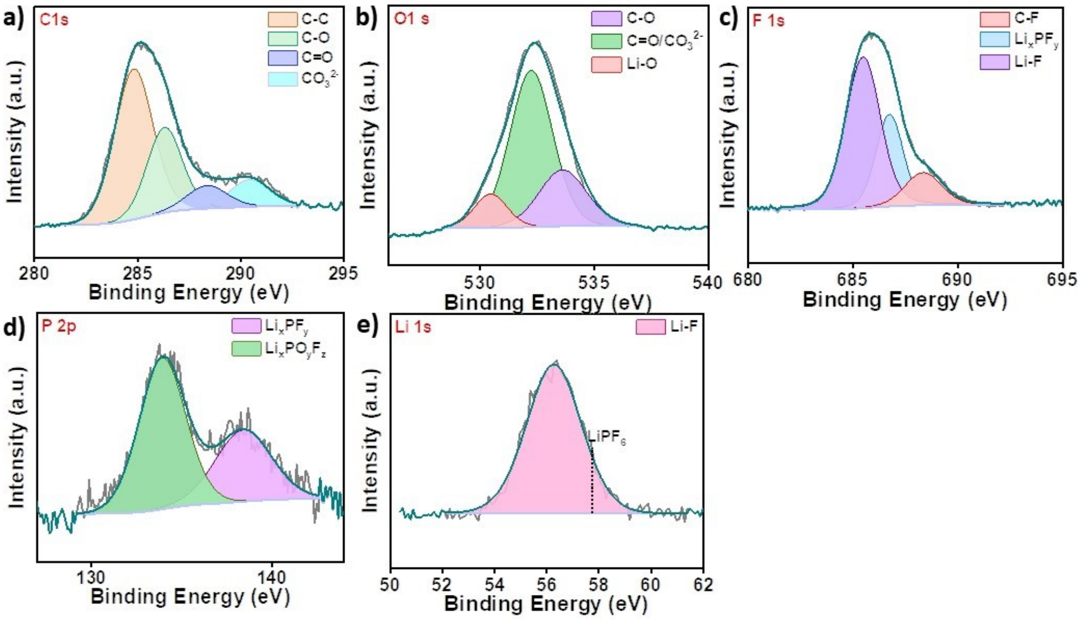

**Figure S29.** XPS spectra BTEG in 1M $LiPF_6$ (EC: DEC) after etch for elements a) C1s, b) O1s, c) F1s, d) P 2p and e) Li 1s.

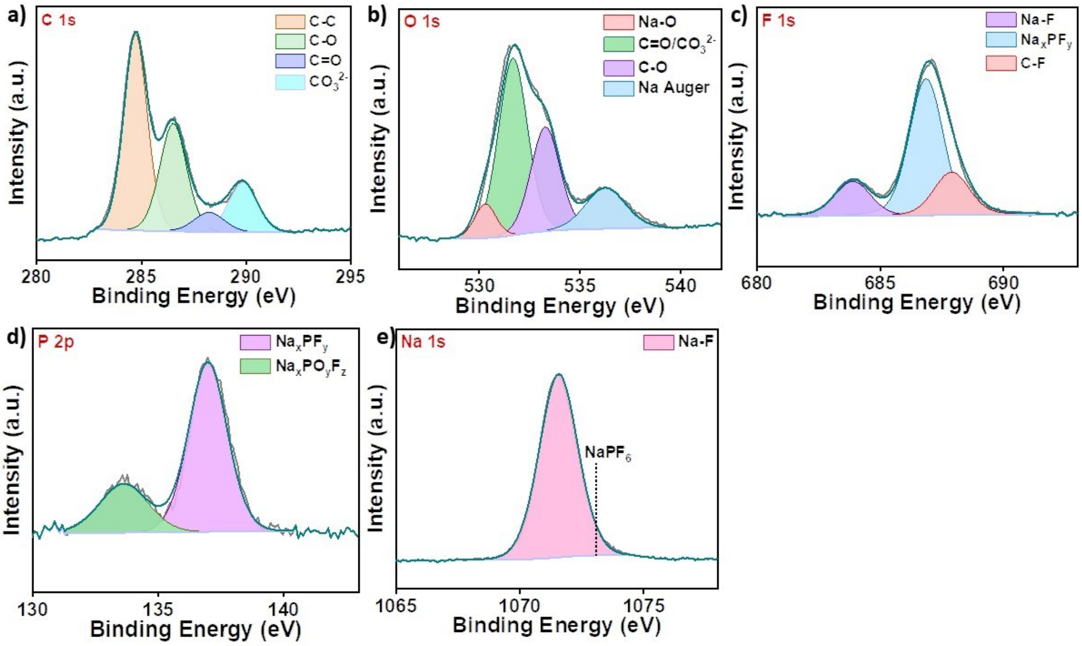

**Figure S30.** XPS spectra BTEG in 1M $NaPF_6$ (EC: DEC) before etch for elements a) C1s, b) O1s, c) F1s, d) P 2p and e) Na 1s.

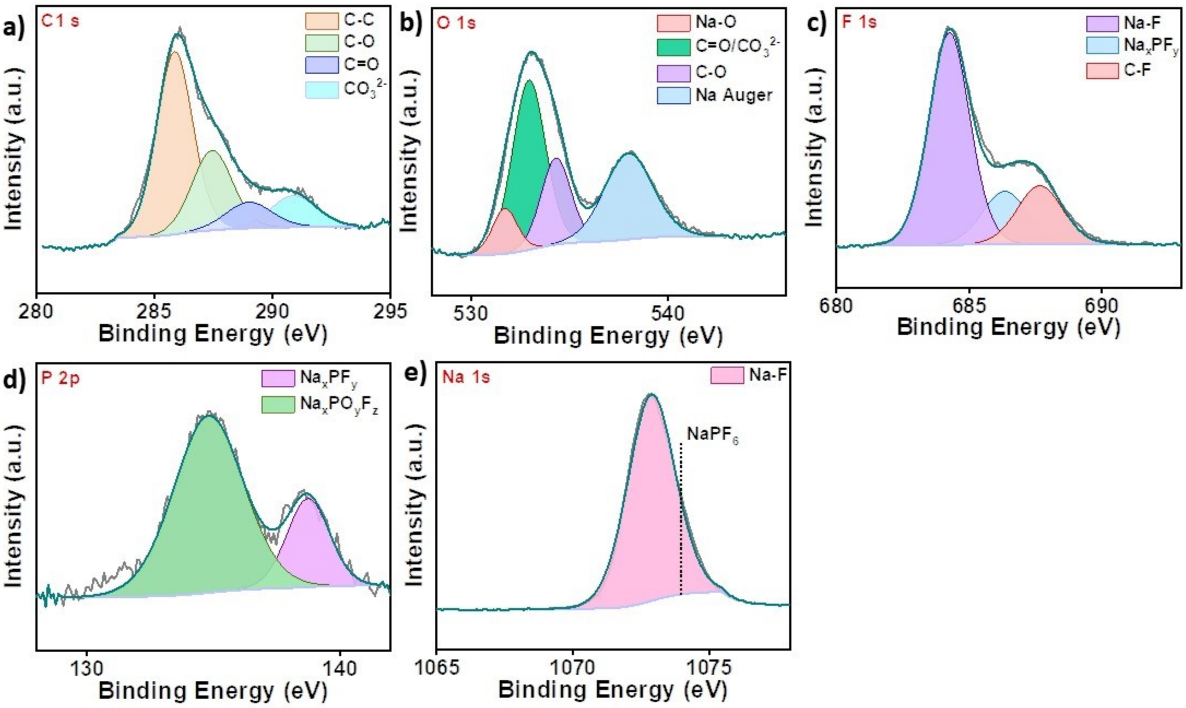

**Figure S31.** XPS spectra BTEG in 1M $NaPF_6$ (EC: DEC) after etch for elements a) C1s, b) O1s, c) F1s, d) P 2p and e) Na 1s.

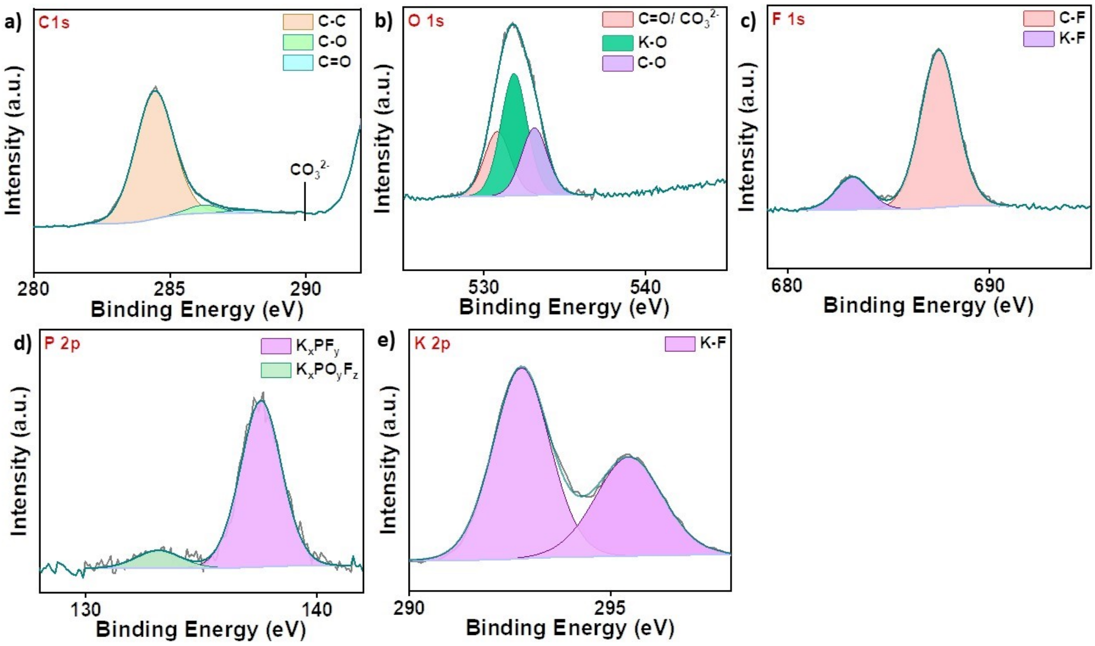

**Figure S32.** XPS spectra BTEG in 0.8M $KPF_6$ (EC: DEC) before etch for elements a) C1s, b) O1s, c) F1s, d) P 2p and e) K 1s.

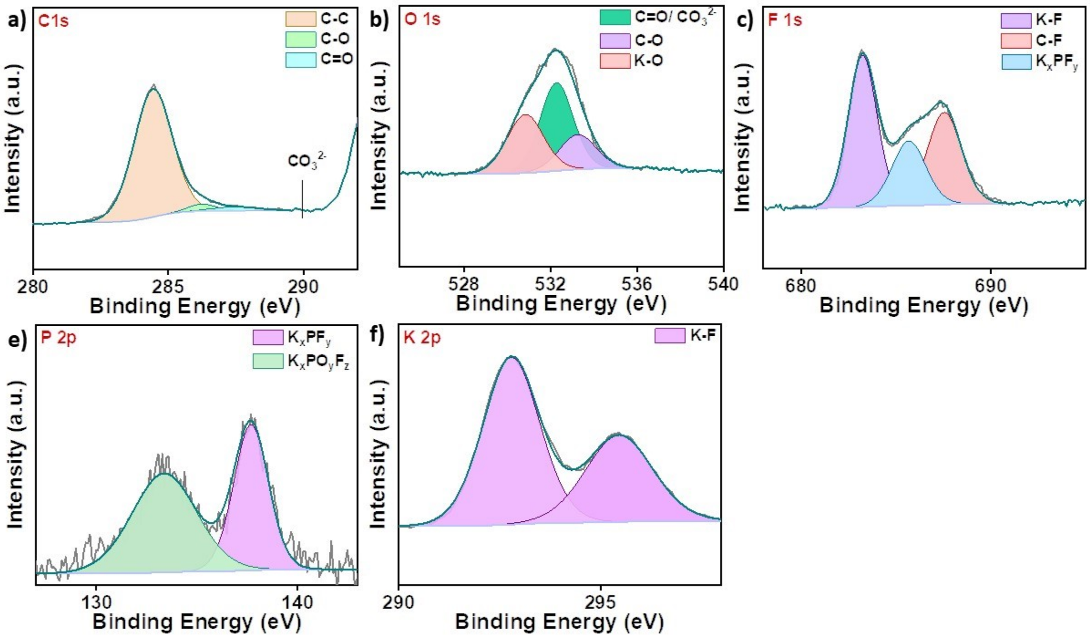

**Figure S33.** XPS spectra BTEG in 0.8M $KPF_6$ (EC: DEC) before etch for elements a) C1s, b) O1s, c) F1s, d) P 2p and e) K 1s.

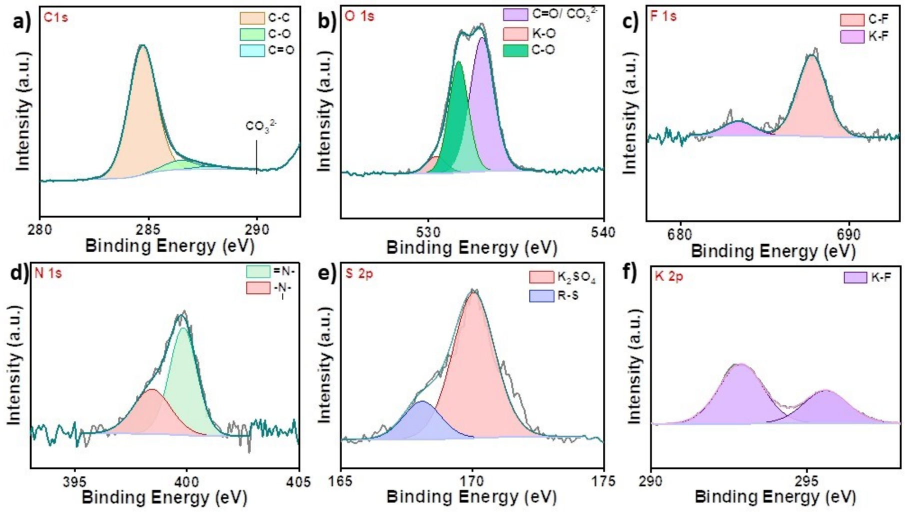

**Figure S34.** XPS spectra BTEG in 1M KFSI (EC: DEC) before etch for elements a) C1s, b) O1s, c) F1s, d) N 1s, e) S 2p and f) K 1s.

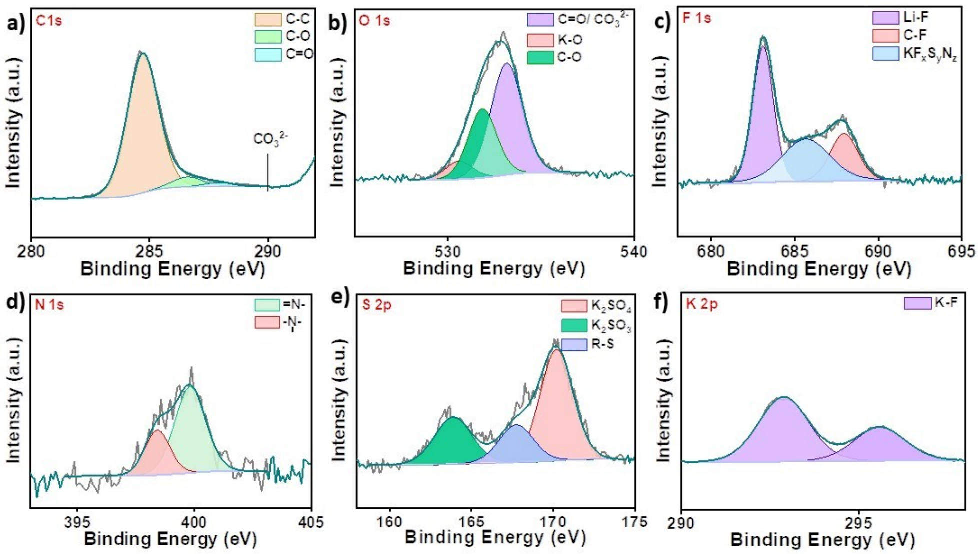

**Figure S35.** XPS spectra BTEG in 1M KFSI (EC: DEC) after etch for elements a) C1s, b) O1s, c) F1s, d) N 1s, e) S 2p and f) K 1s.

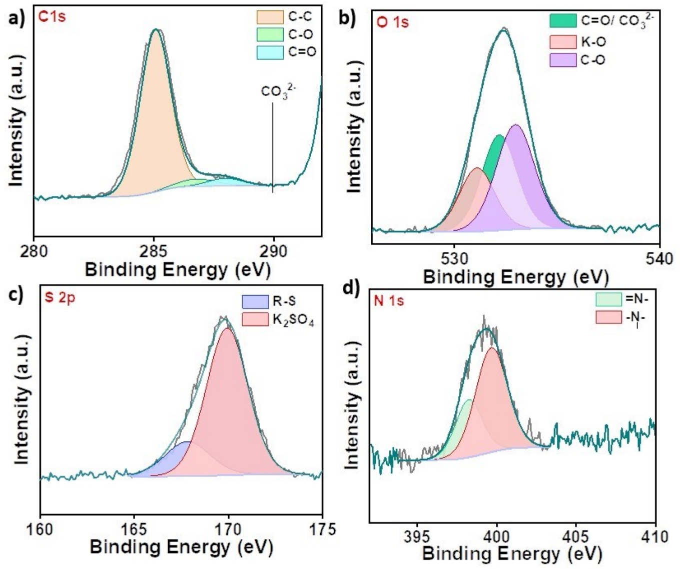

**Figure S36.** XPS spectra BTEG in 5M KFSI (EC: DEC) before etch for elements a) C1s, b) O1s, c) S 2p and d) N 1s.

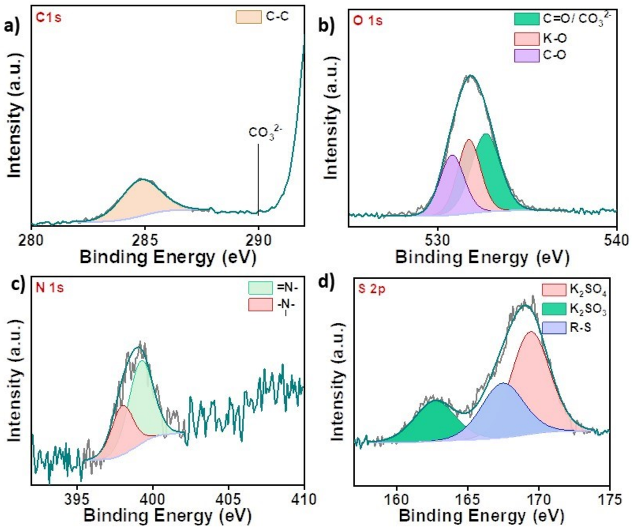

**Figure S37.** XPS spectra BTEG in 5M KFSI (EC: DEC) after etch for elements a) C1s, b) O1s, c) S 2p and d) N 1s.

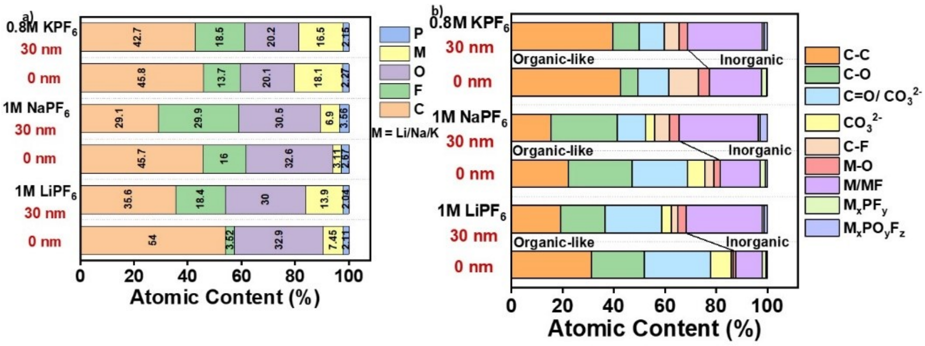

**Figure S38. a)** Elemental contribution (wt. %) in 1M $LiKPF_6$/ $NaKPF_6$ and 0.8M $KPF_6$ in EC: DEC before and after etching, **b)** Organic and inorganic components (wt. %) contribution in 1M $LiPF_6$/ $NaPF_6$ and 0.8 M $KPF_6$ in EC: DEC before and after etching

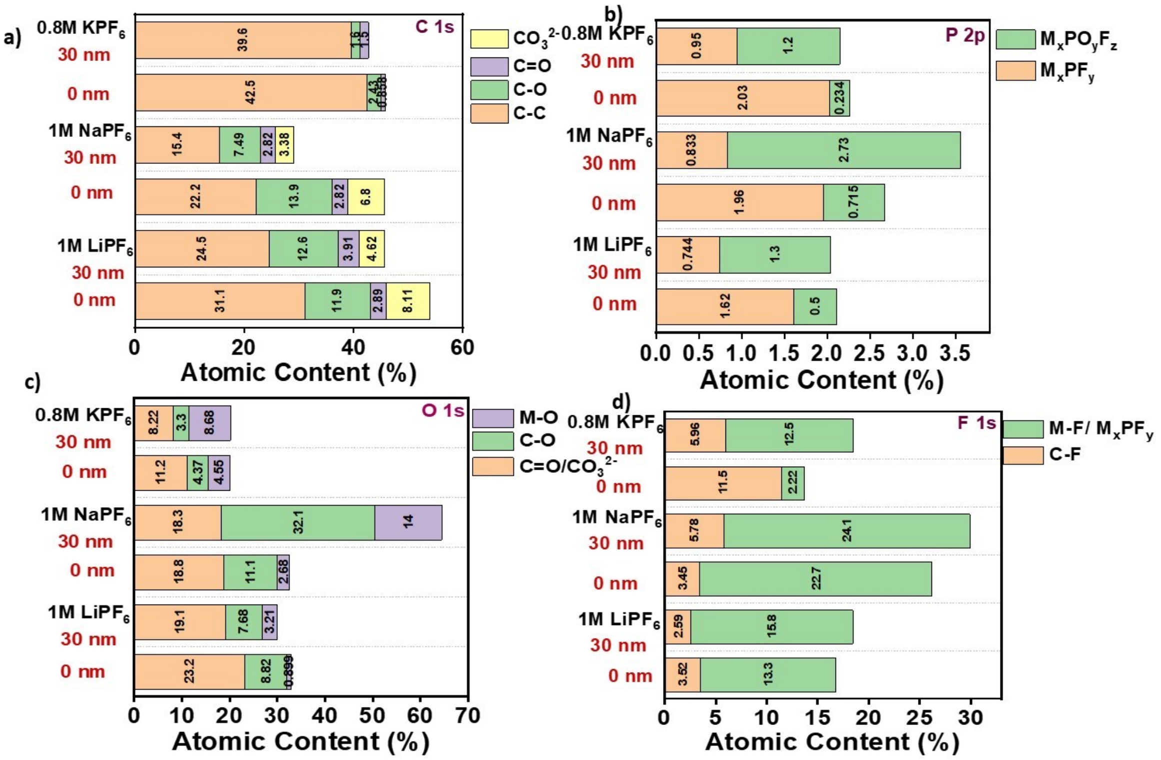

**Figure S39.** Type of species distribution in elements a) C1s, b) P 2p, c) O 1s and d) F 1s for BTEG in 1M Li/ Na/ KPF$_6$ in EC: DEC before and after etching

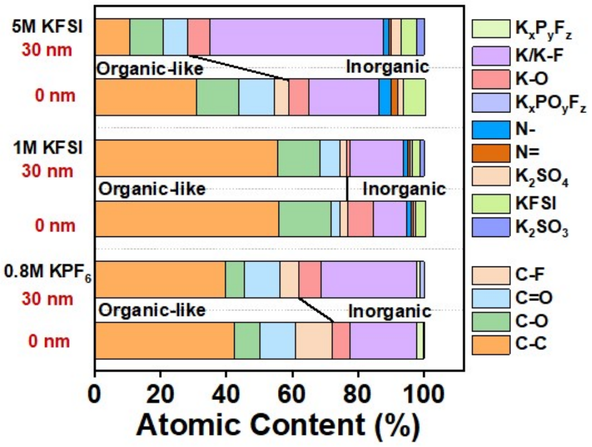

**Figure S40.** Organic and inorganic components (wt. %) contribution in 0.8M KPF$_6$, 1M KFSI and 5M KFSI in EC: DEC before and after etching.

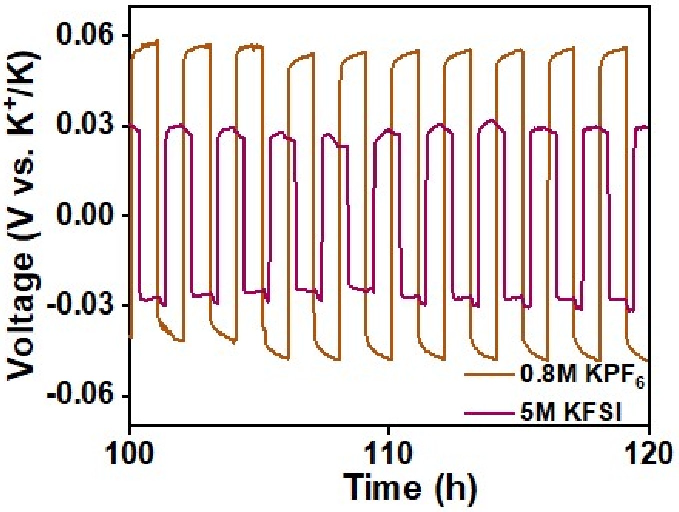

**Figure S41.** Voltage profile of symmetric cell of 0.8M $KPF_6$ and 5MKFSI in EC: DEC after 100 hours.

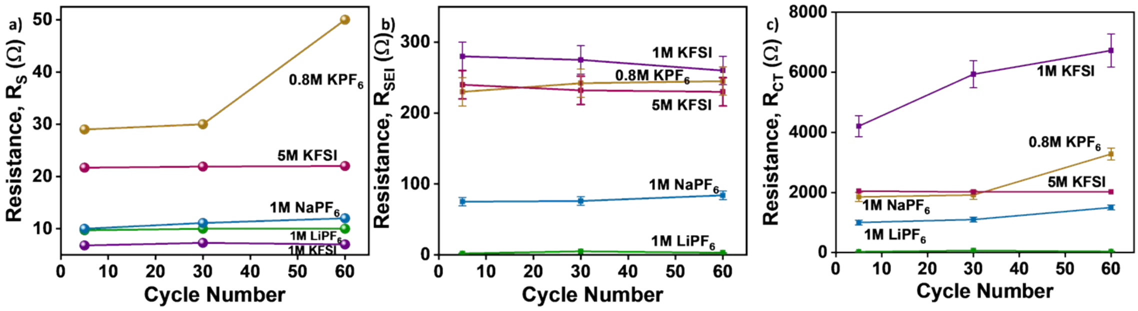

**Figure S42.** Resistance values from a) solution, b) SEI and c) charge transfer derived from equivalent electrical circuit fitting on Nyquist plots.

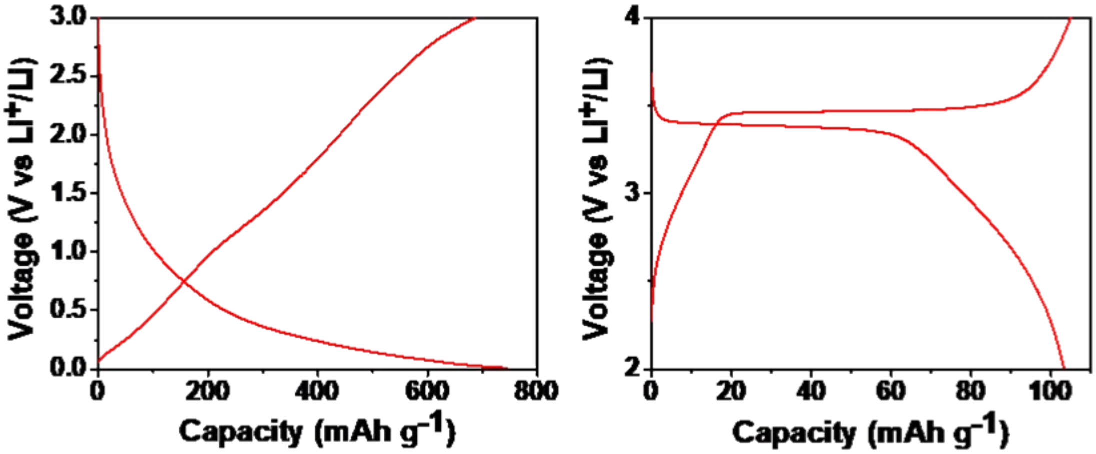

**Figure S43.** Third cycle of charge discharge profile of (a) BTEG at 100 mAg-1 from 0.01V to 3V (b) LFP at C/5 rate from 2V to 4V.

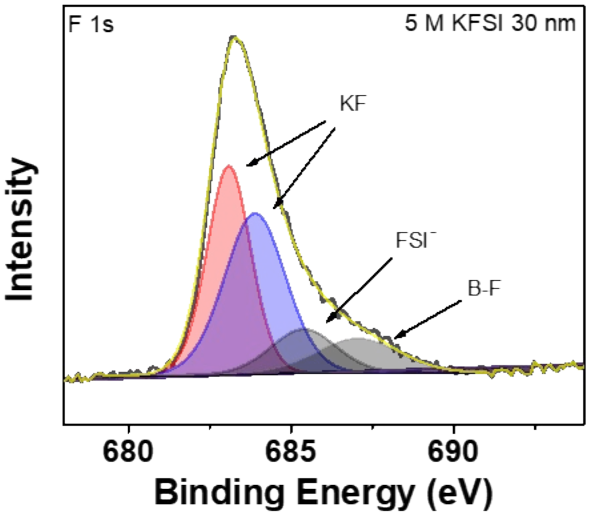

**Figure S44.** Refitted XPS profile of 5 M KFSI at 30 nm etch.

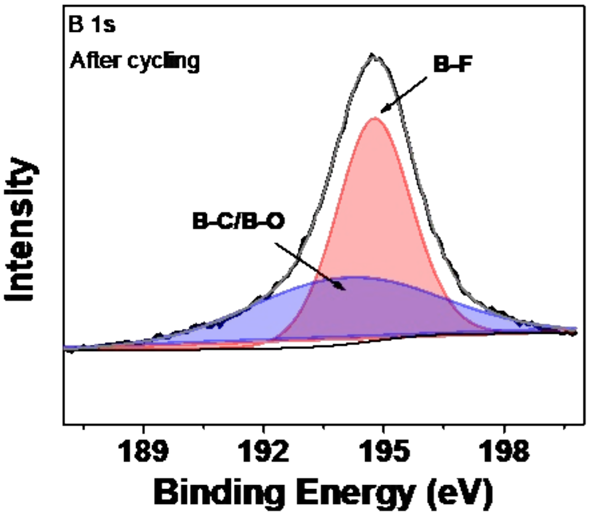

**Figure S45.** B 1s XPS spectra after cycling in 5M KFSI.

**Table 3**. Comparison of electrochemical performance of BTEG anode with the reported literatures

| **Materials (Alkali-ion)** | **Initial reversible capacity (mAh $g^{-1}$) at low current density (mA $g^{-1}$)** | **Cycling capacity (mAh $g^{-1}$) at high current density (A $g^{-1}$)** | **Electrolyte** | **References** |
|---|---|---|---|---|
| **BTEG (LIB)** | 1014 mAh $g^{-1}$ at 25 mA $g^{-1}$ | 276 mAh $g^{-1}$ at 1 A $g^{-1}$ (75% capacity retention after 1000 cycles) | 1M $LiPF_6$ EC:DEC | **OUR WORK** |
| **(SIB)** | 295 mAh $g^{-1}$ at 25 mA $g^{-1}$ | 147 mAh $g^{-1}$ at 1 A $g^{-1}$ (>100% capacity retention after 1000 cycles) | 1M $NaPF_6$ EC:DEC:FEC | |
| **(PIB)** | 369 mAh $g^{-1}$ at 25 mA $g^{-1}$ | 184 mAh $g^{-1}$ at 1 A $g^{-1}$ (87% capacity retention after 1000 cycles) | 5M KFSI EC:DEC | |
| **Fly ash carbon (LIB)** | 376 mAh $g^{-1}$ at 0.1 A $g^{-1}$ | 260.2 mAh $g^{-1}$ to 278 mAh $g^{-1}$ at 1 A $g^{-1}$ for 2000 cycles | 1M $LiPF_6$ EC:DEC | [3] |
| **(SIB)** | 276 mAh $g^{-1}$ at 0.05 A $g^{-1}$ | 158 mAh $g^{-1}$ to 130.6 mAh $g^{-1}$ at 0.4 A $g^{-1}$ for 1000 cycles (82.7% Capacity retention) | 1M $NaPF_6$ EC:DEC | |
| **(PIB)** | 179.5 mAh $g^{-1}$ at 0.05 A $g^{-1}$ | 106.6 mAh $g^{-1}$ to 81.1 mAh $g^{-1}$ at 0.4 A $g^{-1}$ for 2000 cycles (70.1% Capacity retention) | 1M $KPF_6$ EC:DEC | |
| **Cyclized Polyacrylonitrile (LIB)** | 792 mAh $g^{-1}$ at 0.05 A $g^{-1}$ | 810 mAh $g^{-1}$ at 1 A $g^{-1}$ for 1000 cycles (91.8 to 99% capacity retention) | 1M $LiPF_6$ EC:EMC | [4] |
| **(SIB)** | 280 mAh $g^{-1}$ at 0.05 A $g^{-1}$ | SIB and PIB | | |

| | | | | |
|---|---|---|---|---|
| **(PIB)** | 230 mAh g$^{-1}$ at 0.05 mA g$^{-1}$ | stability not shown | | |
| **Crystalline chlorinated contorted hexabenzocoronene (LIB)**<br>**(SIB)**<br>**(PIB)** | 393 mAh g$^{-1}$ at 100 mA g$^{-1}$<br>225 mAh g$^{-1}$ at 20 mA g$^{-1}$<br>260 mAh g$^{-1}$ at 100 mA g$^{-1}$ | 300 mAh g$^{-1}$ at 1 A g$^{-1}$<br>220 mAh g$^{-1}$ at 8 A g$^{-1}$ after 1000 cycles<br>100 mAh g$^{-1}$ after 800 cycles at 1 A g$^{-1}$<br>80 mA g$^{-1}$ at 1 A g$^{-1}$ after 400 cycles | 1.3M LiPF$_6$ in EC:DEC<br>1M NaPF$_6$ in EC:DEC<br>0.8M KPF$_6$ in EC:DEC | [5] |
| **Hard Carbon (LIB)**<br>**(SIB)**<br>**(PIB)** | 429 mAh g$^{-1}$ at 20 mA g$^{-1}$<br>274 mAh g$^{-1}$ at 20 mA g$^{-1}$<br>247 mAh g$^{-1}$ at 20 mA g$^{-1}$ | 76% at 20 mA g$^{-1}$ for 30 cycles<br>93.5% at 20 mA g$^{-1}$ for 30 cycles<br>94.3% at 20 mA g$^{-1}$ for 30 cycles | LiPF$_6$ in EC:PC<br>NaPF$_6$ in EC:PC<br>KPF$_6$ in EC:PC | [6] |
| **Carbon nanoparticles on Ni foam (LIB)**<br>**(SIB)** | 764 mAh g$^{-1}$ at 50 mA g$^{-1}$<br>241 mAh g$^{-1}$ at 50 mA g$^{-1}$ | 664 mAh g$^{-1}$ at 1 A g$^{-1}$ at 500th cycle<br>54 mAh g$^{-1}$ at 1 A g$^{-1}$ (shown for 40 cycles only) | | [7] |
| **Graphitic Nanocarbon (PIB)** | 280 mAh g$^{-1}$ at 50 mA g$^{-1}$ | 189 mAh g$^{-1}$ at 200 mA g$^{-1}$ after 200 cycles | 0.8M KPF$_6$ in EC:DEC | [8] |
| **Crosslinked Hollow Graphitic Carbon (PIB)** | 298 mAh g$^{-1}$ at 50 mA g$^{-1}$ | 269 mAh g$^{-1}$ after 200 cycles | 0.8M KPF$_6$ in EC:DEC | [8] |
| **Sulfur-assisted graphene microspheres (PIB)** | 285 mAh g$^{-1}$ at 50 mA g$^{-1}$ | 95 mAh g$^{-1}$ at 1 A g$^{-1}$; 225 mAh g$^{-1}$ at 200 mA g$^{-1}$ for 1000 cycles | 0.8M KPF$_6$ in EC:EMC | [9] |
| **Graphitic carbon Nanocages (PIB)** | 212 mAh g$^{-1}$ at 0.2 C (55.8 mAh g$^{-1}$, 1C=279 mAh g$^{-1}$) | At 0.2 C for 100 cycles | 1M KFSI in EC:PC | [10] |
| **Boron doped hard carbon (SIB)** | 234 mAh g$^{-1}$ at 30 mA g$^{-1}$ | 180 mAh g$^{-1}$ at 100 mA g$^{-1}$ for 400 cycles | 1M NaPF$_6$ in EC:DEC | [11] |
| **$BC_xO_{3-x}$/C graphite (LIB)** | 403 mAh g$^{-1}$ at 100 mA g$^{-1}$ | 446 mAh g$^{-1}$ at 200 mA g$^{-1}$ for 100 cycles | 1M LiPF$_6$ in EC:DEC | [12] |

| | | | | |
|---|---|---|---|---|
| **Carbon aerogel (SIB)**<br>**(PIB)** | 298 mAh $g^{-1}$ at 0.1 C<br>258 mAh $g^{-1}$ at 0.1 C | 0.03% decay per cycle at 0.5 C for 2000 cycles<br>82.7% at 0.5 C for 1000 cycles | | 13 |
| **Boron doped graphene (LIB)** | 548 mAh $g^{-1}$ at 100 mA $g^{-1}$ | Not shown | 1M $LiPF_6$ EC:DMC | 14 |
| **B/O Biomass derived carbon (PIB)** | 500 mAh $g^{-1}$ at 100 mA $g^{-1}$ | 100 mAh $g^{-1}$ at 1 A $g^{-1}$ after 500 cycles | 0.8M $KPF_6$ EC:DEC | 15 |
| **Boron doped porous carbon (LIB and SIB)** | 600 mAh $g^{-1}$ at 100 mA $g^{-1}$ (LIB) and 300 mA h $g^{-1}$ at 100 mAh $g^{-1}$ (SIB) | 496 mAh $g^{-1}$ at 100 mA $g^{-1}$ after 100 cycles (LIB)<br>180 mAh $g^{-1}$ at 100 mA $g^{-1}$ after 100 cycles (SIB) | 1M $LiPF_6$ EC:DEC:DMC<br>1M $NaClO_4$ EC:DEC:5% FEC | 16 |
| **Boron doped carbon fibres (LIB)** | 370 mAh $g^{-1}$ at 50 mA $g^{-1}$ | 350 mAh $g^{-1}$ at 100 mA $g^{-1}$ for 100 cycles | 1M $LiPF_6$ EC:DEC | 17 |
| **N,S,O co doped hard carbon for (PIB)** | 175 mAh $g^{-1}$ at 100 mA $g^{-1}$ | 136 mAh $g^{-1}$ at 500 mA $g^{-1}$ after 200 cycles | 0.8M $KPF_6$ EC:DEC | 18 |

## References:

1 W. Weppner and R. A. Huggins, *J. Electrochem. Soc.*, 1977, **124**, 1569–1578.

2 J. Kim, S. Park, S. Hwang and W. S. Yoon, *J. Electrochem. Sci. Technol.*, 2021, **13**, 19–31.

3 J. Yin, W. Zhang, G. Huang, N. A. Alhebshi, N. Salah, M. N. Hedhili and H. N. Alshareef, *ACS Appl. Mater. Interfaces*, 2021, **13**, 26421–26430.

4 W. Zhang, M. Sun, J. Yin, E. Abou-Hamad, U. Schwingenschlögl, P. M. F. J. Costa and H. N. Alshareef, *Angewandte Chemie*, 2021, **133**, 1375–1383.

5 K. Eom, M. Kang, J. H. Park, S. H. Joo, J. Park, J. Lee, S. K. Kwak, S. Ahn and S. J. Kang, *J. Mater. Chem. A*, 2021, **9**, 20607–20614.

6 Y. Huang, Y. Wang, P. Bai and Y. Xu, *ACS Appl. Mater. Interfaces*, 2021, **13**, 38441–38449.

7 R. R. Gaddam, N. A. Kumar and X. S. Zhao, *Mater. Today Energy*, 2018, **8**, 29–36.

8 B. Cao, Q. Zhang, H. Liu, B. Xu, S. Zhang, T. Zhou, J. Mao, W. K. Pang, Z. Guo, A. Li, J. Zhou, X. Chen and H. Song, *Adv. Energy Mater.*, DOI:10.1002/aenm.201801149.

9 Q. Zhang, X. Cheng, C. Wang, A. M. Rao and B. Lu, *Energy Environ. Sci.*, 2021, **14**, 965–974.

10 B. Cao, Q. Zhang, H. Liu, B. Xu, S. Zhang, T. Zhou, J. Mao, W. K. Pang, Z. Guo, A. Li, J. Zhou, X. Chen and H. Song, *Adv. Energy Mater.*, DOI:10.1002/AENM.201801149.

11 D. Wu, F. Sun, Z. Qu, H. Wang, Z. Lou, B. Wu and G. Zhao, *J. Mater. Chem. A*, 2022, **10**, 17225–17236.

12 H. Wang, Y. Li, Y. Wang, S. Hu and H. Hou, *J. Mater. Chem. A*, 2017, **5**, 2835–2843.

13 J. Wang, Z. Xu, J. C. Eloi, M. M. Titirici and S. J. Eichhorn, *Adv. Funct. Mater.*, 2022, **32**, 2110862.

14 M. Sahoo, K. P. Sreena, B. P. Vinayan and S. Ramaprabhu, *Mater. Res. Bull.*, 2015, **61**, 383–390.

15 X. Lian, Z. Sun, Q. Mei, Y. Yi, J. Zhou, M. H. Rümmeli and J. Sun, *EEM*, 2022, **5**, 344–352.

16 D. Wang, Z. Wang, Y. Li, K. Dong, J. Shao, S. Luo, Y. Liu and X. Qi, DOI: 10.1016/j.apsusc.2018.09.035.

17 H. Wang, C. Ma, X. Yang, T. Han, Z. Tao, Y. Song, Z. Liu, Q. Guo and L. Liu, DOI: 10.1016/j.solidstatesciences.2015.02.003.

18 M. Chen, Y. Cao, C. Ma and H. Yang, *Nano Energy*, 2021, **81**, 105640.